Acta Crystallographica Section D
Biological Crystallography
ISSN 0907-4449

Structure of the F-spondin reeler domain reveals a unique β-sandwich fold with a deformable disulfide-bonded loop

Masamichi Nagae,[a] Ken Nishikawa,[a] Norihisa Yasui,[a] Motoo Yamasaki,[b] Terukazu Nogi[a] and Junichi Takagi[a]*

[a]Laboratory of Protein Synthesis and Expression, Institute for Protein Research, Osaka University, 3-2 Yamadaoka, Suita, Osaka 565-0871, Japan, and [b]BioFrontier Laboratories, Kyowa Hakko Kogyo Co. Ltd, Asahi-machi 3-6-6, Machida, Tokyo 194-8533, Japan

Correspondence e-mail: takagi@protein.osaka-u.ac.jp

Received 13 June 2008
Accepted 4 September 2008

PDB References: FSP198, 2zot, r2zotsf; FSP145, 2zou, r2zousf.

F-spondin is a secreted and extracellular matrix-attached protein that has been implicated in axonal pathfinding during neural development as well as in vascular remodelling in adult tissues. F-spondin is composed of a reeler, a spondin and six thrombospondin type 1 repeat domains. The reeler domain shares homology with the amino-terminal domain of reelin, a large secreted glycoprotein that guides migrating neurons during cortical development. Crystal structures of the F-spondin reeler domain were determined at 1.45 and 2.70 Å resolution. The structure revealed a nine-stranded antiparallel β-sandwich fold similar to the immunoglobulin or fibronectin type III domains, but with a unique extra β-hairpin. Moreover, an amino-terminal extension which is anchored at its beginning *via* a conserved disulfide bond loosely packs against one face of the β-sandwich, making a major contribution to the surface features of the domain. Structural comparison among the different molecules contained in two different crystals reveals an unusual conformational plasticity of the amino-terminal loop, suggesting its role in molecular interactions.

1. Introduction

F-spondin is a secreted extracellular matrix-attached protein that was originally identified in the floor plate of the rat ventral midline of the embryonic spinal cord using the subtractive hybridization technique (Klar *et al.*, 1992). F-spondin promotes the adhesion and outgrowth of commissural axons *in vitro* and further *in vivo* experiments using recombinant F-spondin and its neutralizing antibody revealed that it is required for accurate pathfinding of commissural axons at the floor plate (Burstyn-Cohen *et al.*, 1999). In contrast, F-spondin inhibits the outgrowth of embryonic motor axons, suggesting its dual role in patterning axonal trajectory in the spinal cord (Tzarfati-Majar *et al.*, 2001). Despite the critical importance of F-spondin in the development of the central nervous system, it is not expressed in adult brain (Miyamoto *et al.*, 2001). Instead, F-spondin is expressed in various organs including the lung, ovary, small intestine and kidney. Surprisingly, F-spondin was purified from adult bovine ovarian follicular fluid and shown to possess growth-promoting activity toward vascular smooth muscle cells (Miyamoto *et al.*, 2001). Furthermore, F-spondin inhibits VEGF- or bFGF-stimulated migration of vascular endothelial cells, pointing toward a possible involvement during angiogenesis (Terai *et al.*, 2001).

F-spondin has 807 amino acids divided into eight domains: an N-terminal reeler domain, a spondin domain and six C-terminal thrombospondin type 1 repeat (TSR) domains. The N-terminal reeler domain of F-spondin shares amino-acid

sequence similarity with reelin, which is an extracellular matrix protein that is involved in brain development (D'Arcangelo *et al.*, 1995; Tissir & Goffinet, 2003). In contrast, the spondin domain is related to the corresponding domain found in mindin, a secreted extracellular protein which has been reported to promote neurite outgrowth from embryonic hippocampal neurons (Feinstein *et al.*, 1999). F-spondin and mindin belong to the same protein family and share two structural domains: spondin and TSR domains.

F-spondin is processed *in vivo* to yield an amino half fragment that includes the reeler and spondin domains and a C-terminal fragment composed of TSR domains (Burstyn-Cohen *et al.*, 1999). Recent studies have shown that the N-terminal fragment binds to the central domain of amyloid-β precursor protein (APP) in a calcium-dependent manner and prevents the initial β-secretase cleavage of APP (Ho & Sudhof, 2004). It is presumed that the interaction with APP is mediated mainly by the spondin domain but not by the reeler domain. In contrast, the C-terminal fragment is comprised of TSR domains that are further processed to produce shorter fragments with opposing biological functions (*i.e.* repulsive and adhesive properties toward neurons); their spatial presentation is controlled by cell-surface receptors that belong to the lipoprotein receptor family (Hoe *et al.*, 2005; Zisman *et al.*, 2007).

While the physiological aspects of F-spondin have been elucidated to a certain extent, only limited information is available concerning its three-dimensional structure. To date, the structures of two TSR domains of F-spondin (TSR-1 and TSR-4) have been solved by NMR spectroscopy (Paakkonen *et al.*, 2006), but no structural information is available for the two N-terminal domains. In this report, we have determined the crystal structures of two different constructs of the F-spondin reeler domain at atomic resolution. Our results reveal that the reeler domain adopts a nine-stranded β-sandwich fold similar to immunoglobulin domains, but it also shows unique structural features including an N-terminal disulfide-bonded loop with unusual structural plasticity.

2. Materials and methods

2.1. Protein preparation and crystallization

The N-terminal 198-residue portion of human F-spondin was amplified from the cDNA (Miyamoto *et al.*, 2001) using primers containing *Not*I and *Xba*I restriction sites. The PCR product was cloned into the *Not*I/*Xba*I site of pcDNA3.1/Myc-His(+) vector (Invitrogen) that had been modified to include a tobacco etch virus (TEV) protease cleavage sequence (ENLYFQG) and His_8 before the Myc tag and His_6 tag. The resultant plasmid (FSP198-tevMycHis) was used to transiently transfect 293T cells using the polyethyleneimine method (Aricescu *et al.*, 2006). The recombinant protein was initially fractionated from the culture supernatant by ammonium sulfate precipitation, which was followed by Ni–NTA agarose chromatography. The crude sample was treated with hexahistidine-tagged TEV protease at room temperature for 16 h and passed through an Ni–NTA agarose column to remove the cleaved tag and the enzyme. The flowthrough fractions were collected for further purification by two column-chromatographic steps on Mono-Q and Superdex200 columns (GE Healthcare), concentrated to 9 mg ml^{-1} and subjected to crystallization. The yield was $\sim$200 µg pure FSP198 per litre of culture supernatant.

Crystallization conditions were searched for with the aid of a Phoenix dispensing robot (Art Robbins Instruments.). Protein solution (0.15 µl) was dispensed into each well of a Corning 96-well plate, mixed with the same volume of precipitant reagent and equilibrated against 100 µl reservoir solution. The initial condition was found from screening using Index Screen (Hampton Research). Optimization of the condition was carried out using the standard-scale hanging-drop vapour-diffusion method. FSP198 crystals of diffraction quality were obtained under conditions consisting of 0.2 *M* bis-tris pH 5.5, 0.4 *M* ammonium acetate, 25% polyethylene glycol (PEG) 3350. The crystals grew in space group $P4_3$, with unit-cell parameters $a = b = 57.6$, $c = 190.9$ Å. A platinum-derivative crystal was obtained by soaking the crystals in a reservoir solution containing 1 m*M* K_2PtCl_4 for 1 d at 293 K.

A truncated construct of the F-spondin reeler domain was designed based on the crystal structure of FSP198. To construct the expression plasmid, a segment corresponding to the domain core (Gly42–Ser186) followed by a stop codon was amplified using primers containing *Bgl*II and *Xba*I sites and cloned into the *Bam*HI/*Xba*I site of pENP4×3 vector. This is a custom-made vector based on pcDNA3.1 which incorporates the signal sequence from mouse nidogen (Takagi *et al.*, 2003) followed by three concatenations of the 'P4' tag sequence (Sangawa *et al.*, 2008) and a TEV site. The resultant plasmid (P4×3tev-FSP145) was used to transiently transfect 293T cells and the expressed protein was directly purified from the culture supernatant using an anti-P4 monoclonal antibody P20.1 coupled to CNBr-activated Sepharose (GE Healthcare). The details of the purification procedure using the P4×3 tag and P20.1 antibody column, together with the vector information, will be published elsewhere (manuscripts in preparation). After the peptide tag had been removed by TEV protease treatment, FSP145 was further purified on a MonoQ column, concentrated to 4.5 mg ml^{-1} and subjected to crystallization. About 200 µg pure FSP145 was obtained from 400 ml culture supernatant.

Initial crystallization conditions were searched for using Index Screen (Hampton Research). After optimization of the initial condition, diffraction-quality crystals were obtained by the hanging-drop vapour-diffusion method under conditions consisting of 0.1 *M* Tris–HCl pH 8.0, 0.2 *M* trimethylamine *N*-oxide and 15% PEG 3350. The crystals grew in space group *C*2, with unit-cell parameters $a = 93.3$, $b = 50.5$, $c = 63.2$ Å, $\beta = 100.4^\circ$.

2.2. Data collection, structure determination and refinement

X-ray diffraction data were collected on beamlines BL-17A and AR-NW12A at Photon Factory, Tsukuba, Japan. All data

Table 1
Data-collection, phasing and refinement statistics.

Values in parentheses are for the highest resolution shell.

Crystal	Native 1 (Fsp198)	Native 2 (Fsp145)	Native 3 (Fsp145)	Pt derivative (Fsp198)
Data-collection statistics				
Space group	$P4_3$	$C2$	$C2$	$P4_3$
Unit-cell parameters (Å, °)	$a = b = 57.6$, $c = 190.9$	$a = 93.3$, $b = 50.5$, $c = 63.2$, $\beta = 100.4$	$a = 93.2$, $b = 50.7$, $c = 63.2$, $\beta = 100.5$	$a = b = 58.5$, $c = 214.2$
Beamline	NW12A, PF-AR	NW12A, PF-AR	NW12A, PF-AR	BL-17A, PF
Wavelength (Å)	1.0000	1.0000	1.7000	1.0723
Resolution (Å)	100–2.70 (2.80–2.70)	100–1.45 (1.50–1.45)	100–1.85 (1.92–1.85)	100–3.10 (3.21–3.10)
Total reflections	49178	179934	172933	88428
Unique reflections	16670	48350	24230	11550
Completeness (%)	97.6 (99.7)	94.5 (93.6)	97.2 (90.2)	88.2 (90.7)
$R_{\rm merge}$ (%)	8.3 (48.8)	6.9 (43.3)	6.0 (25.6)	11.3 (45.6)
$\langle I/\sigma(I)\rangle$	8.6 (2.1)	15.1 (3.3)	11.4 (4.5)	8.2 (5.4)
Phasing statistics				
No. of heavy atoms				7
Phasing power				1.073
Figure of merit (acentric/centric)				0.27/0.13
Refinement statistics				
Resolution range (Å)	57.6–2.70	62.1–1.45		
No. of reflections	15792	45897		
No. of non-H atoms				
Protein	4425	2272		
Water		220		
Others		24		
$R_{\rm work}/R_{\rm free}$† (%)	24.6/31.3	20.3/22.2		
R.m.s. deviations				
Bond lengths (Å)	0.008	0.009		
Bond angles (°)	1.2	1.3		
Mean B factor (Å^2)	39.4	16.0		
Ramachandran plot (%)				
Favoured regions	90.5	96.6		
Allowed regions	8.6	3.4		
Outlier regions	1.3	0.0		

† $R_{\rm free}$ was calculated using 5% of data excluded from refinement.

sets were processed and scaled using the *HKL*-2000 program package (Otwinowski & Minor, 1997). The phases of the FSP198 crystal were determined by the single anomalous dispersion method at 3.1 Å resolution using the platinum derivative with *SHARP*/*autoSHARP* (Vonrhein *et al.*, 2007). Phase improvement and fragment assignment were performed using *RESOLVE* (Terwilliger, 2000). The quality of the electron-density map was good, which allowed us to trace most of the main chain. To phase the native data set (Native 1 in Table 1), molecular replacement was performed using a polyalanine model built with the platinum-derivative data as a search model. Since the unit-cell parameters differed significantly between the native and derivative, positional refinement of the polyalanine model was not successful in phasing the native data set. The calculation was carried out with the program *MOLREP* (Vagin & Teplyakov, 1997) from the *CCP*4 program suite and the phases were extended to 2.7 Å resolution. Further model fitting was performed manually using *XFIT* from *XTALVIEW* (McRee, 1999). Crystallographic refinement was carried out using *CNS* (Brünger *et al.*, 1998) and *REFMAC*5 (Murshudov *et al.*, 1997) from the *CCP*4 program suite. The phases of FSP145 were determined by the molecular-replacement method, using the structure of FSP198 as a search model. The program *MOLREP* was used to calculate the rotation and translation functions. After the initial phase determination, automatic model construction was performed using the *ARP*/*wARP* program (Perrakis *et al.*, 2001). The model-fitting and refinement protocols were the same as those used for FSP198. The quality of the protein models was confirmed with *MOLPROBITY* (Lovell *et al.*, 2003). Data-collection and final refinement statistics are summarized in Table 1. Figures showing molecular structures were prepared using the program *PyMOL* (DeLano Scientific LLC; http://pymol.sourceforge.net). Structural homologues of the F-spondin reeler domain were retrieved from the *DALI* server (Holm & Sander, 1996) and *LSQKAB* and *SSM* (*Secondary Structure Matching*; Krissinel & Henrick, 2004) were used for structural alignment between the proteins.

3. Results

3.1. Structure of FSP198, the longer construct of the F-spondin reeler domain

In order to determine the three-dimensional structure of the F-spondin reeler domain, we first prepared a recombinant fragment corresponding to the N-terminal 198-residue portion of human F-spondin (referred to as FSP198 throughout this manuscript). In order to facilitate detection and purification, an octahistidine tag and a Myc tag were attached at the C-terminus, preceded by a TEV protease cleavage sequence. The protein was purified from the cell-culture supernatant of transiently transfected 293T cells, crystallized and subjected to structural determination by the single anomalous dispersion method using a platinum derivative. In the data-processing step, there were two possibilities for the space group of the FSP198 crystal (*i.e.* $P4_3$ or $P4_32_12$). It was difficult to determine the space group based on data-collection statistics such as the $R_{\rm merge}$ value because the overall $R_{\rm merge}$ values were almost identical (∼8%). Phasing appeared to be successfully completed in both space groups and an interpretable electron-density map was obtained in both cases. However, we found that model refinement did not result in convergence in space group $P4_32_12$, while the crystallographic R factor was significantly reduced when the space group was changed to $P4_3$. It seems that the crystallographic twofold symmetry in $P4_32_12$ is not perfect in this crystal. We therefore concluded that the correct space group was $P4_3$ and processed the data accordingly. With the $P4_3$ setting, the

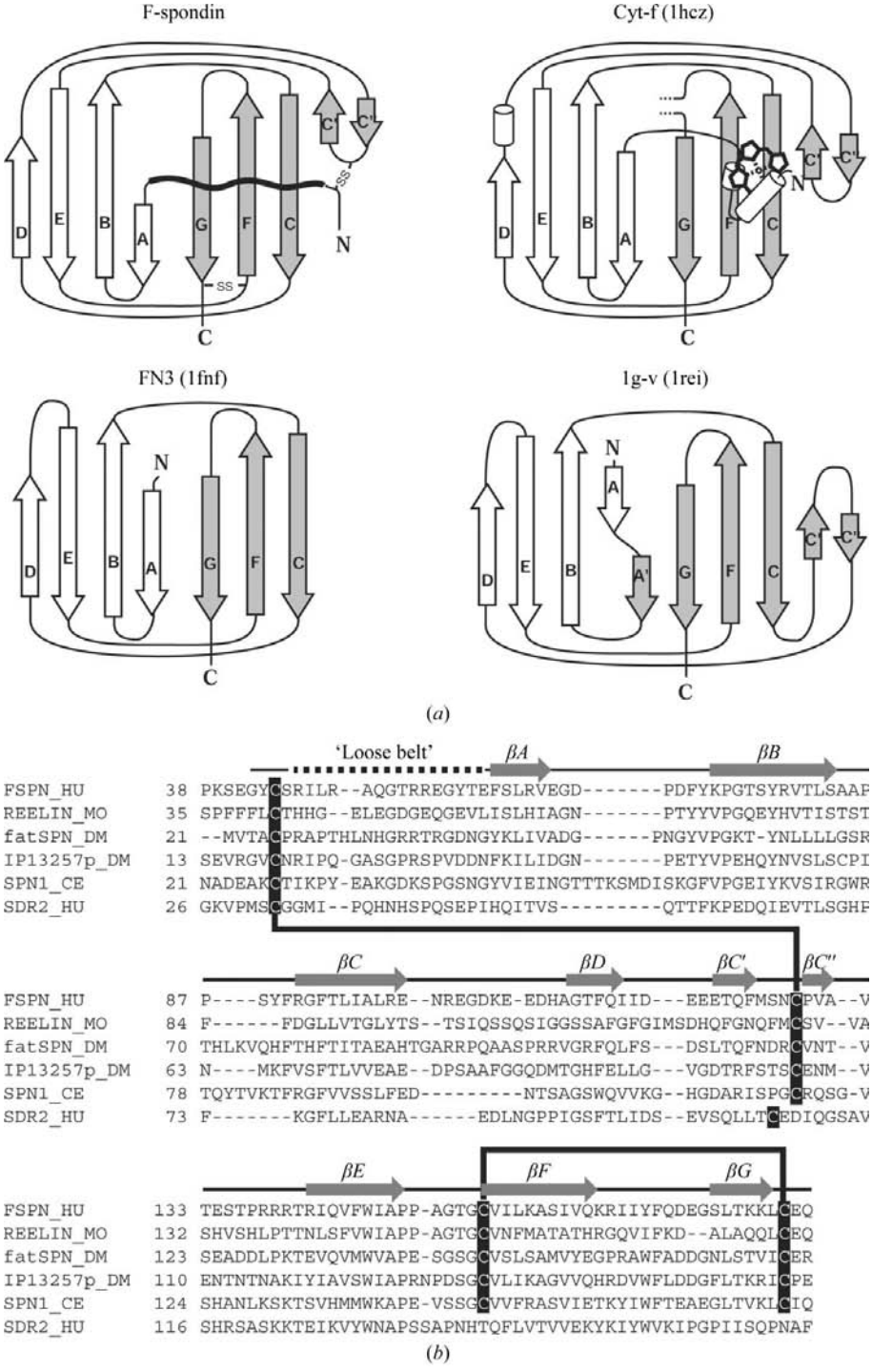

Figure 1
Comparison of the F-spondin reeler domain with other related domains. (*a*) β-Strand topology maps of the F-spondin reeler domain, the cytochrome *f* large domain (Cyt-f; PDB code 1hcz), the fibronectin type III domain (FN3; human fibronectin; PDB code 1fnf) and the V-set Ig domain (Ig-v; 1rei). The 'front' and the 'back' sheets are depicted by grey and white arrows, respectively. The N-terminal loose belt in F-spondin and a haem in cytochrome *f* are represented by thick lines. Note that in F-spondin the *C*′–*C*″ strands follow the *D* rather than the *C* strand in order to conform to the strand-designation convention of other β-sandwiches. (*b*) Multiple sequence alignment of the reeler domains. Sequences are from human F-spondin (FSPN_HU), mouse reelin (REELIN_MO), *Drosophila* fat spondin (fatSPN_DM), *Drosophila* hypothetical protein IP13257p (IP13257p_DM), *Caenorhabditis elegans* spondin-1 (SPN1_CE) and human stromal cell-derived receptor 2 (SDR2_HU). Alignment was performed with *ClustalW* (http://clustalw.genome.jp/). The secondary-structure elements for F-spondin reeler domain are shown above the alignment. The conserved cysteine residues and their connectivity are also indicated.

FSP198 crystal contains four molecules in the asymmetric unit and they are divided into two groups related by imperfect twofold symmetry. We call the two molecules in one group *A* and *B* and those in the other *A*′ and *B*′. While some minor differences occur, these two groups seem to be equivalent in structure. In fact, the deviations between the two groups are very small (0.50 Å r.m.s.d. between *A* and *A*′ and 0.80 Å r.m.s.d. between *B* and *B*′ for the entire molecule). Therefore, only molecules *A* and *B* will be discussed further. As the quality of the electron-density map corresponding to the N-terminal nine residues (29–37, assuming that the mature protein starts with Phe29) and C-terminal 14 residues (185–198) of both molecules was poor, we omitted these segments from the final model. The large ambiguous electron-density map at these segments may have caused the relatively high $R_{\rm free}$ value of FSP198 (Table 1). The crystal structure revealed that the reeler domain of F-spondin is composed of four-stranded (strands *A*, *B*, *E* and *D*) and five-stranded (strands *C*, *F*, *G*, *C*′ and *C*″) antiparallel β-sheets which together form a β-sandwich arrangement (Figs. 1*a* and 2*a*). The outer face of the 'front' sheet (containing strands *CFG*) makes multiple contacts with loops and hence is largely buried, while that of the 'back' sheet (*i.e.* the *ABED* sheet) is completely exposed. Two disulfide bonds, Cys44–Cys128 and Cys156–Cys182, are formed in each monomer. Particularly interesting is the disulfide bridge between Cys44 (the first visible residue of the domain) and Cys128 (located at the tip of the *C*′–*C*″ hairpin), which anchors the N-terminal end of a long flexible loop to the main body of the domain. Although this domain is superficially similar to other common β-sandwich folds such as immunoglobulin (Ig), fibronectin type III (FN3), cytokine receptor family and PKD domains, inspection of the strand topology indicates that it represents a novel variant of these well known folds (Fig. 1*a*).

Surprisingly, molecules *A* and *B* show markedly different conformations in the segment containing the N-terminal loop (Fig. 2*b*, dark colours; Supplementary

Fig. 1). In molecule *A*, the loop makes a long excursion and passes over the ridge of the front sheet at a hydrophobic notch created by the well conserved Tyr170 and Phe171. In contrast, the same loop in molecule *B* shifts downwards by more than 10 Å. The loop now makes a short parallel β-sheet with the Tyr170-Phe171 segment, dragging down the most of the *FG* loop. This difference caused a large r.m.s.d. of 4.2 Å between molecules *A* and *B*, although the r.m.s.d. dropped to 1.3 Å when two segments (37–54 and 165–171) were omitted. Because of the alternative conformation involving the N-terminal loop, molecules *A* and *B* show drastically different surface features at the 'front' side, where a single large electropositive convex region in molecule *A* is deformed into a concave and more neutral platform (Supplementary Fig. 2). In the crystal, these segments in molecule *B* coincide with the packing interface, where residues 164–171 interact extensively with two symmetry-related molecules through van der Waals contacts (data not shown). Therefore, it is possible that the very different loop conformation in molecule *B* is a packing artifact and does not represent the native reeler domain structure.

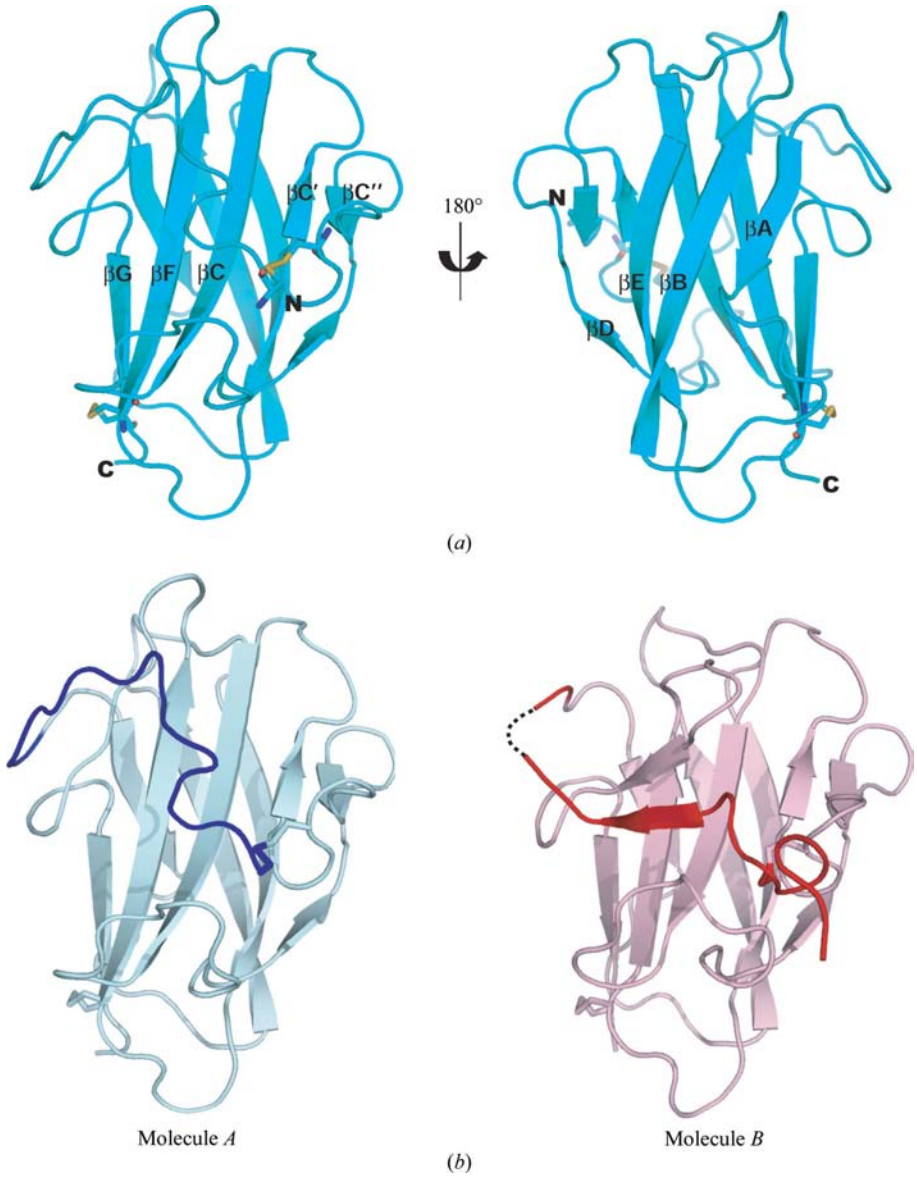

Figure 2
Crystal structure of the F-spondin reeler domain (FSP198). (*a*) Ribbon model of the representative F-spondin reeler domain (molecule *A*) viewed from two different directions. Nine β-strands (βA–βG, $\beta C'$ and $\beta C''$) are labelled as in Fig. 1. Two disulfide bridges are shown as yellow stick models. (*b*) Comparison between the two types of structures present in the crystal. Molecules *A* (cyan) and *B* (magenta) are viewed from the same orientation as the left panel in Fig. 2(*a*). The main body of the domain is in pale colours, while the N-terminal loop is in dark colours. The disordered segment is depicted by a dotted line.

3.2. Structure of FSP145, a truncated construct of the F-spondin reeler domain

The structure of FSP198 described above was of good quality, but the moderate resolution (2.7 Å) and the unexpected structural differences between the two monomers in the asymmetric unit precluded us from unambiguously identifying the actual native structure of this domain. Therefore, we redesigned the expression construct based on the FSP198 structure in order to improve the quality of the crystals. Thus, the largely disordered N-terminal and C-terminal segments were removed, leaving the core 145-residue portion (Gly42–Ser186, referred to as FSP145). Furthermore, the new construct contained a novel affinity-tag sequence (P4×3 tag; Nogi *et al.*, manuscript in preparation) at its N-terminus followed by a TEV protease cleavage sequence. This N-terminal tagging is ideal because TEV cleavage leaves only two residues (Gly-Ser) derived from the vector at the N-terminus. Indeed, the redesigned fragment behaved very well and crystallized readily in multiple conditions. One crystal diffracted to 1.45 Å resolution and the structure was determined by molecular replacement using the coordinates obtained for FSP198 (Table 1; Fig. 3*a*). The FSP145 crystal contained two molecules in the asymmetric unit. The electron density was excellent for the most part of both molecules, with the exception of the N-terminal loop region (Fig. 3*b*). In order to distinguish them from the molecules in the FSP198 crystal, the two monomers were designated molecules *C* and *D*. Although the N-terminal loop segment (Leu48–Arg54) of

[1] Supplementary material has been deposited in the IUCr electronic archive (Reference: MH5017). Services for accessing this material are described at the back of the journal.

molecule *C* was omitted from the final model, it was possible to build a reasonable model for the same segment in molecule *D* because of the presence of continuous and traceable electron density (Supplementary Fig. 2). With this high resolution, side-chain rotamers could be resolved for 18 of the 275 residues of the two independent molecules. Most of the residues were located on the molecular surface and were distributed rather evenly throughout the surface. Therefore, the presence of conformational rotamers in molecules *C* and *D* does not seem to correlate with the structural plasticity seen between molecules *A* and *B*.

The anomalous difference Fourier map calculated from the data set at a wavelength of 1.7000 Å (Native 3 in Table 1) revealed five strong peak densities above 3.5σ corresponding to S atoms from one methione residue (Met125) and two disulfide bridges per monomer (Fig. 3*b*). Because of this unambiguous assignment of the Cys44–Cys128 disulfide position, we could build a model for the first five residues of the N-terminal loop (Tyr43–Ile47) for molecule *C*.

Structural comparison revealed that the protein structures of the two monomers were essentially identical, with an r.m.s.d. value of 0.59 Å for all C^{α} atoms (except for the residues that were missing in molecule *C*). When superposed onto the FSP198 structures, it became evident that molecules *C* and *D* shared the same structure as molecule *A*, but showed significant deviation from that of molecule *B* (Fig. 4*a*). Therefore, we conclude that different conformations of loops and strands observed in molecule *B* are the product of packing deformations rather than being an alternative physiological conformation and the authentic native structure of the F-spondin reeler domain is represented by molecules *A*, *C* and *D*. Nonetheless, the easily deformable nature of the front face of the β-sandwich observed in molecule *B* may be relevant to its biological function.

Although the N-terminal loop was visible in molecule *D*, its conformation was again greatly different from that in molecule *A* (Fig. 4*a* and Supplementary Fig. 1). From the starting Cys44, the loop in molecule *D* (gold) wraps around the front face of the *CFG* sheet as in molecule *A* (blue), but with a different path. The loop does not pack against the hydrophobic ridge of the front sheet, but instead makes a salt bridge between the flipped Glu56 and Arg167. As a result, this loop segment (Ser45–Gly57) shows a surprisingly large r.m.s.d. of 3.6 Å between molecules *A* and *D*. The unusual flexibility of this segment is further underscored by the lack of the clear electron density in molecule *C* (green).

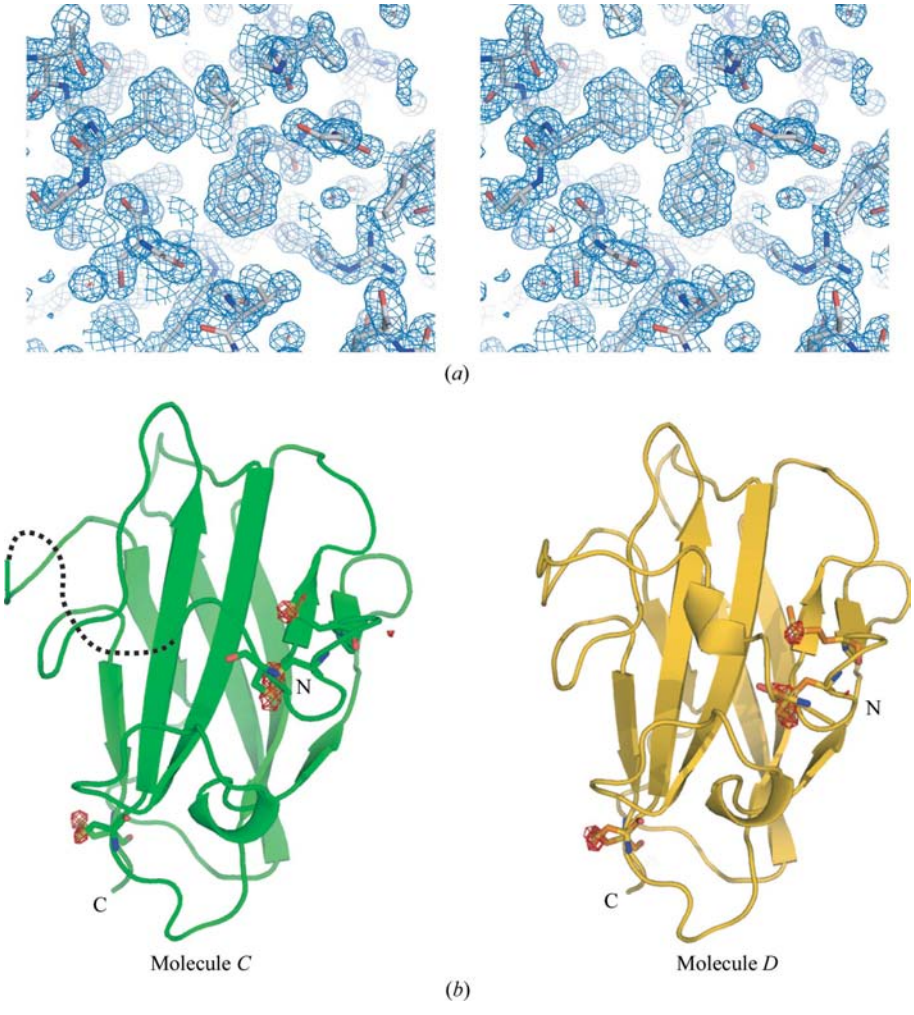

Figure 3
Structure of FSP145. (*a*) Stereo diagram of the weighted $2|F_o| - |F_c|$ electron-density map near Phe90. (*b*) Ribbon models of two monomers in the asymmetric unit (molecule *C*, green; molecule *D*, gold) viewed from the same orientation as in Fig. 2(*b*) are shown. The anomalous difference Fourier map calculated from the Native 3 data in Table 1 contoured at 3.5σ is shown as a red mesh.

4. Discussion

The reeler domain is present in several extracellular proteins including F-spondin, reelin and stromal cell-derived receptor 2 (SDR-2; Shirozu *et al.*, 1996; Fig. 1*b*). There are more than 80 protein sequences listed in the Pfam database that contain the reeler domain. Although some of these proteins are specifically expressed in neural tissues, no specific biological function has been attributed to this domain. The present study reports the first structural determination of this domain. The overall structure revealed an antiparallel β-sandwich similar to fibronectin type III or immunoglobulin domains (Fig. 2*a*). The presence of the extra C'–C'' strand is reminiscent of the V-set Ig domain (Fig. 1*a*), but the fundamental difference in strand topology argues against a possible evolutional relationship. In fact, the reeler domain is quite

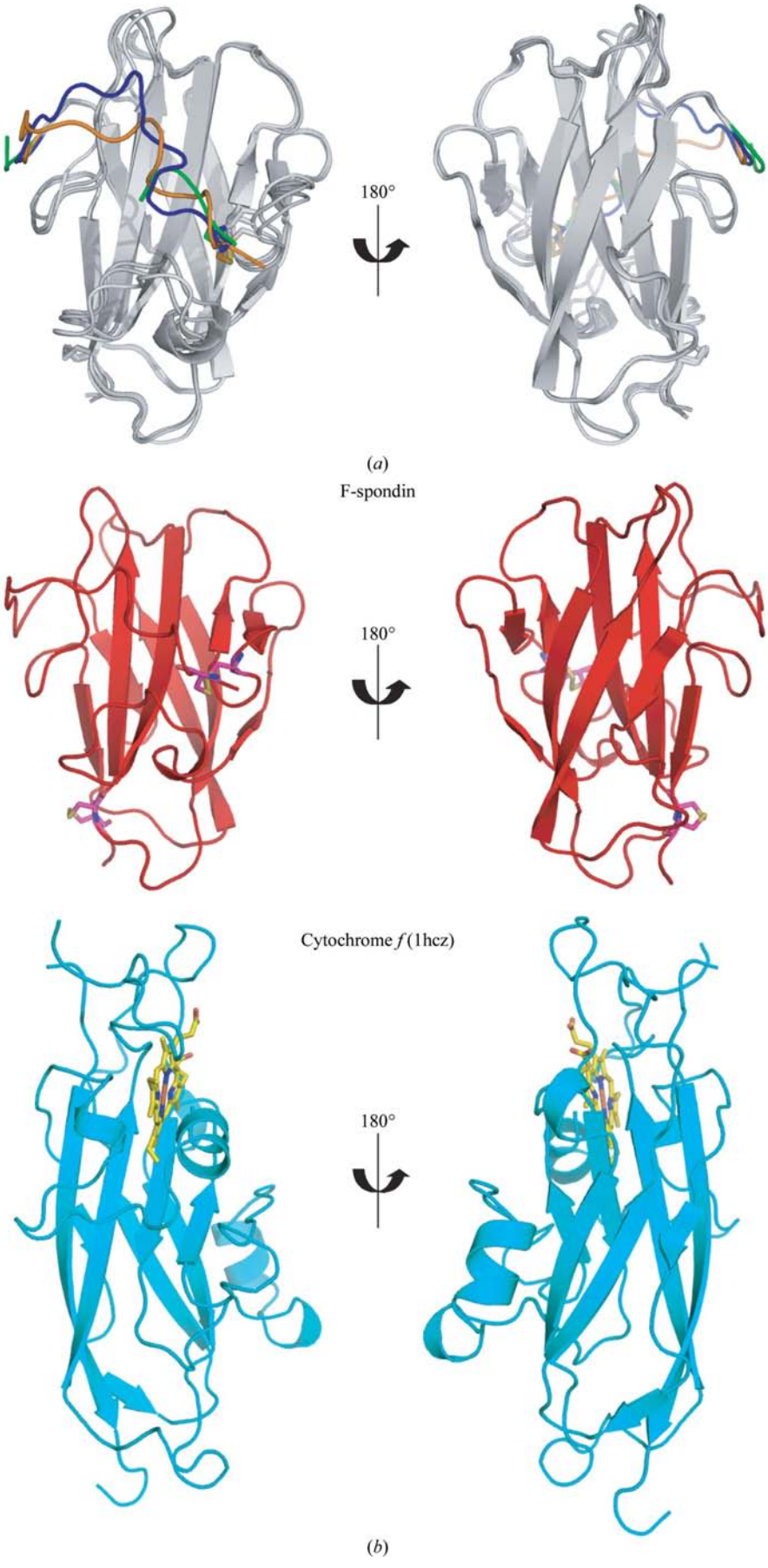

unique in that the 'front' side of the β-sandwich (*i.e.* the *CFG* sheet) is decorated by the N-terminal flexible loop and the long curled *CD* loop, while the 'back' side of the *ABED* sheet is completely exposed to solvent. Because of this feature, the reeler domain is generally much longer (~150 residues) than typical FN3 and Ig domains (~100 residues).

The most unusual structural feature of the reeler domain reported here is the presence of a highly mobile loop at the N-terminus. This loop is not a strand-connecting loop nor does it protrude from the core antiparallel β-sandwich. It is disulfide-bonded at one end and loosely wraps around the 'front' sheet. We decided to call this loop region a 'loose belt' because the first six residues (Ser45–Ala50) in molecules *A* and *D* do not interact with the core β-sandwich domain. The ability of the loose belt to assume widely differing conformations indicates the structural plasticity of the front surface of the reeler-domain β-sandwich.

Structural comparisons of the F-spondin reeler domain using the *DALI* server resulted in a surprising top hit with the lumen-side domains of cytochrome *f* (PDB code 1hcz; *Z* score = 8.0). The lumen-side domain of cytochrome *f*, a subunit of the proton-pumping cytochrome b_6f complex in photosynthetic membranes, is composed of two structural domains (Martinez *et al.*, 1996). The large domain consists of a nine-stranded antiparallel β-sandwich, whereas the small β domain contains 63 amino-acid residues and is inserted in the middle of the *G* strand of the large domain. Despite the low sequence identity (~18%) and differences in the length of

Figure 4
(*a*) Various conformations of the N-terminal 'loose belt' loop. The segment corresponding to Cys44–Tyr58 of molecules *A* (blue), *C* (green) and *D* (gold) shows widely different conformations, while the remainders of the molecules (grey) are virtually superimposable. (*b*) Structural comparison between the F-spondin reeler domain (red) and the luminal domain of cytochrome *f* (blue; PDB code 1hcz). In the cytochrome *f* structure, the inserted small domain is removed for clarity and the haem is shown as a stick model.

the loops, the β-sandwich core of the F-spondin reeler domain has essentially the same fold as the cytochrome *f* large domain (Fig. 4*b*). Importantly, the two short N-terminal helices of cytochrome *f* holding the redox-centre haem are situated at the 'front' side of the *CFG* sheet in a roughly equivalent position to the loose belt of the reeler domain (Figs. 4*b* and 1*a*). Within this structural class, therefore, it may be possible that unique functionality has been incorporated at the front side using the N-terminal segment during evolution.

5. Conclusion

The crystal structure of the F-spondin reeler domain reveals a β-sandwich fold in which the N-terminal loop region exhibits an unusually high flexibility. The N-terminal end of this mobile loop is covalently anchored by a disulfide bond *via* conserved cysteine residues. The overall domain fold, although similar to those of Ig, FN3 and other related domains, is unique in that one of the two outer faces of the β-sandwich is covered by loops, suggesting a specialized function of this face in mediating protein–protein interactions.

We thank Keiko Tamura-Kawakami, Emiko Mihara and Maiko Nampo for excellent technical assistance. We also thank Drs N. Igarashi, N. Matsugaki and Y. Yamada for providing the data-collection facilities and for support. This work was supported in part by the 'Target Proteins Research Program (TPRP)' grant from the Ministry of Education, Culture, Sports, Science and Technology of Japan (MEXT) and by the Protein 3000 Project grant from MEXT.

References

Aricescu, A. R., Lu, W. & Jones, E. Y. (2006). *Acta Cryst.* D**62**, 1243–1250.
Brünger, A. T., Adams, P. D., Clore, G. M., DeLano, W. L., Gros, P., Grosse-Kunstleve, R. W., Jiang, J.-S., Kuszewski, J., Nilges, M., Pannu, N. S., Read, R. J., Rice, L. M., Simonson, T. & Warren, G. L. (1998). *Acta Cryst.* D**54**, 905–921.
Burstyn-Cohen, T., Tzarfaty, V., Frumkin, A., Feinstein, Y., Stoeckli, E. & Klar, A. (1999). *Neuron*, **23**, 233–246.
D'Arcangelo, G., Miao, G. G., Cheng, S. C., Soares, H. D. & Morgen, J. I. & Curran, T. (1995). *Nature (London)*, **374**, 719–723.
Feinstein, Y., Borrell, V., Garcia, C., Burstyn-Cohen, T., Tzarfaty, V., Frumkin, A., Nose, A., Okamoto, H., Higashijima, S., Soriano, E. & Klar, A. (1999). *Development*, **126**, 3637–3648.
Ho, A. & Sudhof, T. C. (2004). *Proc. Natl Acad. Sci. USA*, **101**, 2548–2553.
Hoe, H. S., Wessner, D., Beffert, U., Becker, A. G., Matsuoka, Y. & Rebeck, G. W. (2005). *Mol. Cell. Biol.* **25**, 9259–9268.
Holm, L. & Sander, C. (1996). *Methods Enzymol.* **266**, 653–662.
Klar, A., Baldassare, M. & Jessell, T. M. (1992). *Cell*, **69**, 95–110.
Krissinel, E. & Henrick, K. (2004). *Acta Cryst.* D**60**, 2256–2268.
Lovell, S. C., Davis, I. W., Arendall, W. B., de Bakker, P. I., Word, J. M., Prisant, M. G., Richardson, J. S. & Richardson, D. C. (2003). *Proteins*, **50**, 437–450.
Martinez, S. E., Huang, D., Ponomarev, M., Cramer, W. A. & Smith, J. L. (1996). *Protein Sci.* **5**, 1081–1092.
McRee, D. E. (1999). *J. Struct. Biol.* **125**, 156–165.
Miyamoto, K., Morishita, Y., Yamazaki, M., Minamino, N., Kangawa, K., Matsuo, H., Mizutani, T., Yamada, K. & Minegishi, T. (2001). *Arch. Biochem. Biophys.* **390**, 93–100.
Murshudov, G. N., Vagin, A. A. & Dodson, E. J. (1997). *Acta Cryst.* D**53**, 240–255.
Otwinowski, Z. & Minor, W. (1997). *Methods Enzymol.* **276**, 307–326.
Paakkonen, K., Tossavainen, H., Permi, P., Rakkolainen, H., Rauvala, H., Raulo, E., Kilpelainen, I. & Guntert, P. (2006). *Proteins*, **64**, 665–672.
Perrakis, A., Harkiolaki, M., Wilson, K. S. & Lamzin, V. S. (2001). *Acta Cryst.* D**57**, 1445–1450.
Sangawa, T., Nogi, T. & Takagi, J. (2008). In the press.
Shirozu, M., Tada, H., Tashiro, K., Nakamura, T., Lopez, N. D., Nazarea, M., Hamada, T., Sato, T., Nakano, T. & Honjo, T. (1996). *Genomics*, **37**, 273–280.
Takagi, J., Yang, Y., Liu, J.-H., Wang, J.-H. & Springer, T. A. (2003). *Nature (London)*, **424**, 969–974.
Terai, Y., Abe, M., Miyamoto, K., Koike, M., Yamasaki, M., Ueda, M., Ueki, M. & Sato, Y. (2001). *J. Cell. Physiol.* **188**, 394–402.
Terwilliger, T. C. (2000). *Acta Cryst.* D**56**, 965–972.
Tissir, F. & Goffinet, A. M. (2003). *Nature Rev. Neurosci.* **4**, 496–505.
Tzarfati-Majar, V., Burstyn-Cohen, T. & Klar, A. (2001). *Proc. Natl Acad. Sci. USA*, **98**, 4722–4727.
Vagin, A. & Teplyakov, A. (1997). *J. Appl. Cryst.* **30**, 1022–1025.
Vonrhein, C., Blanc, E., Roversi, P. & Bricogne, G. (2007). *Methods Mol. Biol.* **364**, 215–230.
Zisman, S., Marom, K., Avraham, O., Rinsky-Halivni, L., Gai, U., Kligun, G., Tzarfaty-Majar, V., Suzuki, T. & Klar, A. (2007). *J. Cell Biol.* **178**, 1237–1249.